Acta Mech 228, 129–140 (2017)
DOI 10.1007/s00707-016-1701-7

ORIGINAL PAPER

K. F. Wang · B. Wang · C. Zhang

Surface energy and thermal stress effect on nonlinear vibration of electrostatically actuated circular micro-/nanoplates based on modified couple stress theory

Received: 11 January 2016 / Revised: 29 April 2016 / Published online: 13 August 2016

Abstract Electrostatically actuated circular micro-/nanoplates are commonly used in micro-/nanoswitches and pumps. This paper models the thermal and size effects on the nonlinear vibration behavior of electrostatically actuated circular micro-/nanoplates. Surface elasticity and modified couple stress theories are simultaneously applied to the modeling. A reduced-order model incorporating temperature change is derived and solved numerically. Results show that the material length scale, surface energy, negative temperature change, and geometry nonlinear strain increase frequency and pull-in voltage of the plate. However, Casimir force and positive temperature change reduce the frequency of the plate. Moreover, the effects of surface energy, material length scale and temperature change on frequency become more obvious for thinner plates. The influence of the geometrically nonlinear strain on the frequency is significant for large initial gap to thickness ratio of the plate.

1 Introduction

Electrostatically actuated micro-/nanodevices are used as transistors, switches, pressure sensors, and pumps. An electrostatically actuated switch is generally comprised of a conductive deformation electrode and a rigid grounded electrode [1]. Applied direct current (DC) voltage between the two electrodes leads to bending of the deformable electrode. Once the superimposition of an alternating current (AC) and DC voltage is applied across the two electrodes, harmonic motions of the system will occur, and the system can be used as resonant devices. The natural frequency of the system is affected by the deflection of the deformable electrode. Such devices have wide applications in signal filtering [2], pressure sensors [3], pumps [4], and chemical and mass sensing [5].

With continuing reduction in size, the molecular interaction forces between the two electrodes, such as Casimir force and van der Waals force, become increasingly significant and should be considered. At micro-/nanoscales, the molecular interaction forces between the two electrodes lead the deformable electrode deflects, and affect the frequency of the deformable electrode. When the gap between the two electrodes is smaller than the plasma wavelength (typically below 20 nm), molecular interaction is generally described by van der Waals force. On the other hand, for a larger gap (typically larger than 20 nm), the Casimir force is commonly used to

K. F. Wang (✉) · B. Wang
Graduate School at Shenzhen, Harbin Institute of Technology, Harbin 150001, People's Republic of China
E-mail: wangkaifa@126.com

C. Zhang
School of Civil Engineering, Qingdao University of Technology, Qingdao 266033, People's Republic of China

B. Wang · C. Zhang
Institute for Infrastructure Engineering, Western Sydney University, Penrith, NSW 2751, Australia

describe the molecular interactions between the two electrodes [6]. Ramezani et al. [6] investigated the pull-in instability of cantilever switches subjected to intermolecular and electrostatic forces. Jia et al. [7,8]studied the pull-in instability and free vibration of geometrically nonlinear microswitches under electrostatic and Casimir force. Batra et al. [9–11] investigated the influence of the molecular interactions on the pull-in instability and frequencies of clamped rectangular, circular, and elliptic plates. Wang et al. [12] investigated the pull-in instability and the vibration for a prestressed circular electrostatically actuated plate with consideration of the Casimir force. However, those studies [6–12] did not consider the size-dependent behavior of micro-/nanoscale structures.

At micro-/nanoscale, the properties of micro-/nanomaterials are size dependent, due to the effects of surface energy and material length scale. In practice, the surface energy effect can be described by surface elasticity theory provided by Gurtin and Murdoch [13]. Using this theory, some researchers have found that surface energy plays an important role in the frequencies of nanostructures [14–16]. For example, Fu and Zhang [14] studied the influence of the surface energies on the static and dynamic responses of nanoswitches. On the other hand, the modified couple stress theory provided by Yang et al. [17] can accurately describe the effects of material length scale constants and was widely used to investigate the size-dependent behavior of microbeams [18,19] and microplates [20].

Since surface elasticity theory describes the surface property and modified couple stress theory describes the effect of material length scale in the bulk, it is natural to combine both of them in investigating mechanical behaviors of micro-/nanostructures. For example, the combined effects of surface energy and material length scale on static and dynamic behaviors of nanobeams [21,22] and nanoplates [23] are studied. Unfortunately, there are few reports on the combined effects of surface energy and the material length scale on the mechanical behaviors of electrostatically actuated micro-/nanoplates. Wang et al. [24]investigated the combined effects of surface energy and the material length scale on the pull-in voltage of a rectangular micro-/nanoplate. However, they did not consider a thermal effect. In fact, micro-/nanodevices can be subjected to temperature changes during device packaging and sensing operation [25]. Some researchers have discussed the influence of temperature changes on the pull-in instability and vibration of electrostatically actuated beams [26,27] and plates [10,28]. In these studies, it is found that with a moderate temperature increase devices may premature fail.

Circular plates are commonly electrostatically actuated in many MEMS/NEMS devices, such as switches [29,30] and pumps [4]. Moreover, surface energy, material length scale, and temperature change have significant effect on the performance of electrostatically actuated MEMS/NEMS. Therefore, in this paper, the nonlinear dynamical behaviors of electrostatically actuated circular micro-/nanoplates incorporating thermal and surface energy effects are studied by using modified couple stress theory. The paper is organized as follows: Sect. 2 derives the nonlinear motion equations of a circular plate, based on the modified coupled stress theory. Section 3 derives the reduced-order models for the circular plate. Section 4 gives numerical results and discusses some important factors, such as surface energy, material length scale, geometrically nonlinear deformation, Casimir force and temperature change, which may affect the fundamental frequency of the circular plate. Conclusions are drawn in Sect. 5.

2 Derivation of the nonlinear motion equations

As shown in Fig. 1, an electrostatically actuated micro-/nanodevice including a pair of parallel circular plates is considered. The upper circular electrode is treated as a deformable elastic circular plate with radius R and thickness h. The other one is a rigid and grounded plate. The initial gap between the two plates is g_0. At the center of the mid-plane of the upper plate, a cylindrical coordinate system (r, φ, z) is introduced, whereas the r axis, φ axis and z axis are, respectively, taken along the radius, the tangential, and the depth (thickness) directions of the plate. The upper and lower surfaces of the deformable plate are, respectively, denoted by $S^+(z = h/2)$ and $S^-(z = -h/2)$. For an axisymmetric problem, the displacement components are independent of φ and can be written as

$$u_r = u_r^0 - z\frac{\partial w}{\partial r}, \quad u_\varphi = 0 \quad \text{and } w = w(r) \tag{1}$$

where u_r, u_φ and w are the displacements along the r axis, φ axis and z axis, respectively. u_r^0 is the displacement along the r axis at mid-plane ($z = 0$). Taking the van Kármán strain into consideration, the strains can be expressed as

$$\varepsilon_r = u_{r,r} + \frac{1}{2}w_{,r}^2 \quad \text{and } \varepsilon_\varphi = \frac{u_r}{r}. \tag{2}$$

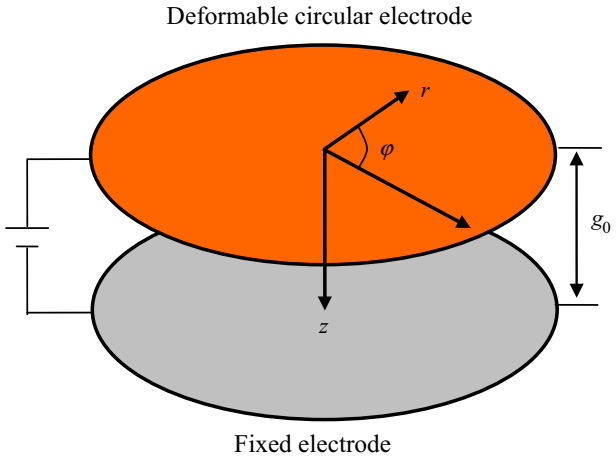

Fig. 1 Sketch of the electrostatically actuated circular micro-/nanoplate

The symmetric curvature tensors of the circular plate are

$$\theta_\theta = -\frac{\partial w}{\partial r}, \quad \chi_{r\theta} = \frac{1}{2}\left(\frac{1}{r}\frac{\partial w}{\partial r} - \frac{\partial^2 w}{\partial r^2}\right). \tag{3}$$

Taking the temperature change ΔT into consideration, the stress can be expressed as

$$\sigma_r = \frac{E}{1+\nu}\left(\varepsilon_{rr} + \frac{\nu}{1-\nu}(\varepsilon_{rr} + \varepsilon_{\varphi\varphi})\right) - \frac{E\alpha_\mathrm{T}\Delta T}{1-\nu}, \tag{4}$$

$$\sigma_\varphi = \frac{E}{1+\nu}\left(\varepsilon_{\varphi\varphi} + \frac{\nu}{1-\nu}(\varepsilon_{rr} + \varepsilon_{\varphi\varphi})\right) - \frac{\alpha_\mathrm{T}\Delta T}{1-\nu}, \tag{5}$$

$$m_{r\varphi} = 2\frac{El_\mathrm{c}^2}{2(1+\nu)}\chi_{r\varphi} \tag{6}$$

where E and ν are the Young's module and Poisson's ratio, respectively, l_c denotes the material length scale in the context of modified coupled stress theory, α_T is thermal coefficient of the plate. Based on the modified couple stress theory, the strain energy in the bulk of the micro-/nanoplate is

$$U_b = \frac{1}{2}\int\int\int (\sigma_r\varepsilon_r + \sigma_\varphi\varepsilon_\varphi + 2m_{r\varphi}\chi_{r\varphi})r\mathrm{d}r\mathrm{d}\varphi\mathrm{d}z. \tag{7}$$

For a different surface element with length dr and width dφ, its area after deformation is given by

$$\mathrm{d}s = \left[1 + \frac{\partial u}{\partial r} + \frac{1}{2}\left(\frac{\partial w}{\partial r}\right)^2\right]\left[1 + \frac{u_r}{r}\right]r\mathrm{d}r\mathrm{d}\varphi. \tag{8}$$

Assuming that the properties of the upper and lower surfaces are isotropic, the surface energy can be expressed as [31]

$$\gamma = \gamma_0 + \frac{1}{2}\left[\lambda_s\left(\varepsilon^s_{\alpha\alpha}\right)^2 + 2\mu_\mathrm{s}\left(\varepsilon^s_{\alpha\beta}\varepsilon^s_{\alpha\beta}\right)\right] \tag{9}$$

where γ_0 is the initial surface energy (or the residual surface stress), λ_s and μ_s are two Láme constants of the surface layer, and $\varepsilon^s_{\alpha\beta}$ denotes the strain tensor of the surface layer.

The total surface energy can be calculated by $U_s = \int_s \gamma\mathrm{d}s$. Using Eqs. (8) and (9), and neglecting the higher term, the total energy of upper and lower surface layers can be obtained,

$$U_s = 2\int\int \gamma_0\left[1 + \frac{\partial u_r^0}{\partial r} + \frac{u_r^0}{r} + \frac{1}{2}\left(\frac{\partial w}{\partial r}\right)^2\right]r\mathrm{d}r\mathrm{d}\varphi + \int\int\frac{1}{2}\left(\sigma^{s^+}_{\alpha\beta}\varepsilon^{s^+}_{\alpha\beta} + \sigma^{s^-}_{\alpha\beta}\varepsilon^{s^-}_{\alpha\beta}\right)r\mathrm{d}r\mathrm{d}\varphi, \tag{10}$$

where $\sigma_{\alpha\beta}^{s+}$ and $\varepsilon_{\alpha\beta}^{s+}$ are the surface stress and surface strain of the surface layer S^+, and $\sigma_{\alpha\beta}^{s-}$, and $\varepsilon_{\alpha\beta}^{s-}$ are the surface stress and surface strain of the surface layer S^-.

When an applied voltage V is applied cross the two plates, by neglecting fringing fields, the electrostatic force can be expressed as [1]

$$F_e = \frac{\varepsilon_0 V^2}{2(g_0 - w)^2} \tag{11}$$

where ε_0 is the dielectric constant of vacuum.

In this Section, the interaction molecule force between the two plates is described by Casimir force and can be expressed as [32,33]

$$F_C = \frac{\bar{h}c\pi^2}{240(g_0 - w)^4} \tag{12}$$

where c is the speed of light in vacuum and $\bar{h}$ is Planck's constant. Therefore, the potential energy due to electrostatic and Casimir force is

$$W_q = -\int\int\int_0^w q\mathrm{d}w r\mathrm{d}r\mathrm{d}\varphi \tag{13}$$

where $q = F_e + F_C$. The kinetic energy of the plate can be expressed as

$$T = \frac{\rho h}{2}\int_{t_0}^{t_1}\int\int\left[\left(\frac{\partial w}{\partial t}\right)^2 + \left(\frac{\partial u}{\partial t}\right)^2\right] r\mathrm{d}r\mathrm{d}\varphi\mathrm{d}t \tag{14}$$

where ρ is the mass density of the plate. The rule of Hamilton's principle requires $\delta\int_{t_0}^{t_1}(U_b + U_s + W_q - T) = 0$, hence one obtains

$$\frac{1}{r}\left[\frac{\partial(rN_{rr}^*)}{\partial r} - N_{\varphi\varphi}^*\right] - I\ddot{u}_r^0 = 0 \tag{15.1}$$

$$\frac{1}{r}\frac{\partial^2(rM_{rr}^*)}{\partial r^2} - \frac{\partial M_{\varphi\varphi}^*}{\partial r} + 2\gamma_0\frac{\partial}{\partial r}\left(r\frac{\partial w}{\partial r}\right) + \frac{\partial}{\partial r}\left(rN_{rr}^*\frac{\partial w}{\partial r}\right) + q - I\ddot{w} = 0. \tag{15.2}$$

In Eq. (15), $N_{rr}^* = N_{rr} + N_{rr}^s$, $N_{\varphi\varphi}^* = N_{\varphi\varphi} + N_{\varphi\varphi}^s$, $M_{rr}^* = M_{rr} + M_{rr}^s + Y_{r\varphi}$, $M_{\varphi\varphi}^* = M_{\varphi\varphi} + M_{\varphi\varphi}^s - Y_{r\varphi}$, where

$$N_{rr} = \int_{-h/2}^{h/2}\sigma_{rr}\mathrm{d}z = \frac{Eh}{1-\nu^2}\left[\frac{\partial u_r^0}{\partial r} + \frac{1}{2}\left(\frac{\partial w}{\partial r}\right)^2 + \frac{\nu u_r^0}{r}\right] - \frac{Eh\alpha_\mathrm{T}\Delta T}{1-\nu}, \tag{16.1}$$

$$N_{\varphi\varphi} = \int_{-h/2}^{h/2}\sigma_{\varphi\varphi}\mathrm{d}z = \frac{Eh}{1-\nu^2}\left[\nu\left(\frac{\partial u_r^0}{\partial r} + \frac{1}{2}\left(\frac{\partial w}{\partial r}\right)^2\right) + \frac{u_r^0}{r}\right] - \frac{Eh\alpha_\mathrm{T}\Delta T}{1-\nu}, \tag{16.2}$$

$$M_{rr} = \int_{-h/2}^{h/2}\sigma_{rr}z\mathrm{d}z = -D\left(\frac{\partial^2 w}{\partial r^2} + \frac{\upsilon}{r}\frac{\partial w}{\partial r}\right), \tag{16.3}$$

$$M_{\varphi\varphi} = \int_{-h/2}^{h/2}M_{\varphi\varphi}\mathrm{d}z = -D\left(\frac{1}{r}\frac{\partial w}{\partial r} + \upsilon\frac{\partial^2 w}{\partial r^2}\right), \tag{16.4}$$

$$N_{rr}^s = \sigma_{rr}^{s+} + \sigma_{rr}^{s-} = \frac{2E^s}{1-\nu^2}\left[\frac{\partial u_r^0}{\partial r} + \frac{1}{2}\left(\frac{\partial w}{\partial r}\right)^2 + \frac{\nu u_r^0}{r}\right] - \frac{E^s\alpha_\mathrm{T}\Delta T}{1-\nu}, \tag{16.5}$$

$$N_{\varphi\varphi}^s = \sigma_{\varphi\varphi}^{s+} + \sigma_{\varphi\varphi}^{s-} = \frac{2E^s}{1-\nu^2}\left[\nu\left(\frac{\partial u_r^0}{\partial r} + \frac{1}{2}\left(\frac{\partial w}{\partial r}\right)^2\right) + \frac{u_r^0}{r}\right] - \frac{E^s\alpha_\mathrm{T}\Delta T}{1-\nu}, \tag{16.6}$$

$$M_{rr}^s = \frac{h}{2}\sigma_{rr}^{s+} - \frac{h}{2}\sigma_{rr}^{s-} = -\frac{E^s h^2}{2(1-\nu^2)}\left(\frac{\partial^2 w}{\partial r^2} + \frac{\nu}{r}\frac{\partial w}{\partial r}\right), \tag{16.7}$$

$$M_{\varphi\varphi}^s = \frac{h}{2}\sigma_{\varphi\varphi}^{s+} - \frac{h}{2}\sigma_{\varphi\varphi}^{s-} = -\frac{E^s h^2}{2(1-\nu^2)}\left(\frac{1}{r}\frac{\partial w}{\partial r} + \nu\frac{\partial^2 w}{\partial r^2}\right), \tag{16.8}$$

$$Y_{r\varphi} = -\frac{El_\mathrm{c}^2 h}{2(1+\nu)}\left(\frac{\partial^2 w}{\partial r^2} - \frac{1}{r}\frac{\partial w}{\partial r}\right) \tag{16.9}$$

where E^s is Young's modulus of surface, $D = Eh^3/12(1-\nu^2)$. Accordingly, the boundary conditions are:

$$(N^*_{rr} + 2\gamma_0) r\delta u_r|_0^R = 0, \tag{17.1}$$

$$\left(M^*_{rr} r\delta \frac{\partial w}{\partial r}\right)|_0^R = 0, \tag{17.2}$$

$$\left\{\frac{\partial}{\partial r}(M^*_{rr} r) - M^*_{\varphi\varphi} - \left[(N^*_{rr} + 2\gamma_0)\frac{\partial w}{\partial r} r\right]\right\} \delta w|_0^R = 0. \tag{17.3}$$

Using Eqs. (15) and (16), the following equations can be obtained:

$$\begin{aligned} &D^*\nabla^4 w - \left(2\gamma_0 + \tfrac{(Eh+2E^s)\alpha_T \Delta T}{1-\nu}\right)\nabla^2 w + \rho h \tfrac{\partial^2 w}{\partial t^2} - q \\ &- \tfrac{E^* h}{1-\nu^2}\left\{\left(\tfrac{\partial^2 w}{\partial r^2} + \tfrac{1}{r}\tfrac{\partial w}{\partial r}\right) L(w, u_r) + \tfrac{\partial w}{\partial r}\tfrac{\partial}{\partial r} L(w, u_r)\right\} = 0, \end{aligned} \tag{18.1}$$

$$\frac{E^* h}{1-\nu^2}\left[\frac{\partial^2 u_r^0}{\partial r^2} + \frac{1}{r}\frac{\partial u_r^0}{\partial r} - \frac{u_r^0}{r^2} + \frac{\partial w}{\partial r}\frac{\partial^2 w}{\partial r^2} + \frac{1-\nu}{2r}\left(\frac{\partial w}{\partial r}\right)^2\right] = \rho h \frac{\partial^2 u_r^0}{\partial t^2} \tag{18.2}$$

where $D^* = \frac{Eh^3}{12(1-\nu^2)} + \frac{E_s h^2}{2(1-\nu^2)} + \frac{(Eh+2E_s)l_c^2}{2(1+\nu)}$, $L(w, u_r) = \left(\frac{\partial u_r^0}{\partial r} + \frac{1}{2}(\frac{\partial w}{\partial r})^2 + \nu\frac{u_r^0}{r}\right)$ and $E^* = E + \frac{2E^s}{h}$.

By introducing the following dimensionless parameters: $\bar{r} = \frac{r}{R}, \bar{w} = \frac{w}{g_0}, \alpha = \frac{g_0^2}{h^2}, \beta_s = \frac{2\gamma_0 R^2}{D}, \lambda = \frac{\varepsilon_0 V^2 R^4}{2Dg_0^3}$, $\mu = \frac{\bar{h} c \pi^2 R^4}{240 D g_0^5}, \tau^2 = \frac{\rho h R^4}{D}, \bar{t} = \frac{t}{\tau}$ $\bar{u}_r^0 = \frac{u_r^0 R}{g_0^2}, \vartheta = \frac{h^2}{6R^2}, \chi = \frac{E_s}{Eh}, \bar{l}_c = (1-\nu)(\frac{l_c}{h})^2$, and $\beta_T = 12(1+\nu)(1+2\chi)(\frac{R}{h})^2\alpha_T\Delta T$, Eq. (18) can be expressed in another form:

$$\begin{aligned} &\ddot{\bar{w}} + (1 + 6\chi + \bar{l}_c)\nabla^4\bar{w} - (\beta_s - \beta_T)\nabla^2\bar{w} - 12\alpha(1+2\chi) \\ &\times\left\{\left(\tfrac{\partial^2\bar{w}}{\partial\bar{r}^2} + \tfrac{1}{\bar{r}}\tfrac{\partial\bar{w}}{\partial\bar{r}}\right) L(\bar{w}, \bar{u}_r^0) + \tfrac{\partial\bar{w}}{\partial\bar{r}}\tfrac{\partial}{\partial\bar{r}} L(\bar{w}, \bar{u}_r^0)\right\} - \tfrac{\lambda}{(1-\bar{w})^2} - \tfrac{\mu}{(1-\bar{w})^4} = 0, \end{aligned} \tag{19.1}$$

$$\frac{\vartheta}{1+2\chi}\frac{\partial^2\bar{u}_r^0}{\partial\tau^2} - \left[\frac{\partial^2\bar{u}_r^0}{\partial\bar{r}^2} + \frac{1}{\bar{r}}\frac{\partial\bar{u}_r^0}{\partial\bar{r}} - \frac{\bar{u}_r^0}{\bar{r}^2} + \frac{\partial\bar{w}}{\partial\bar{r}}\frac{\partial^2\bar{w}}{\partial\bar{r}^2} + \frac{1-\nu}{2\bar{r}}\left(\frac{\partial\bar{w}}{\partial\bar{r}}\right)^2\right] = 0 \tag{19.2}$$

where $L(\bar{w}, \bar{u}_r^0) = \left(\frac{\partial\bar{u}_r^0}{\partial\bar{r}} + \frac{1}{2}(\frac{\partial\bar{w}}{\partial\bar{r}})^2 + \nu\frac{\bar{u}_r^0}{\bar{r}}\right)$. In this Section, only the vibration of the z-axis is considered. Neglecting the inertial term in Eq. (19.2), one obtains

$$\frac{\partial^2\bar{u}_r^0}{\partial\bar{r}^2} + \frac{1}{\bar{r}}\frac{\partial\bar{u}_r^0}{\partial\bar{r}} - \frac{\bar{u}_r^0}{\bar{r}^2} + \frac{\partial\bar{w}}{\partial\bar{r}}\frac{\partial^2\bar{w}}{\partial\bar{r}^2} + \frac{1-\nu}{2\bar{r}}\left(\frac{\partial\bar{w}}{\partial\bar{r}}\right)^2 = 0. \tag{20}$$

The boundary conditions for a clamped circular micro-/nanoplate are

$$\bar{u}_r^0 = 0 \ \text{ and } \ \bar{w} = \frac{\partial\bar{w}}{\partial\bar{r}} = 0. \tag{21}$$

3 Reduced-order model

It is difficult to find a closed-form solution of the nonlinear equations. Therefore, approximate solutions of the displacements $\bar{w}$ and $\bar{u}_r^0$ are constructed as

$$\bar{w}(\bar{r}, \bar{t}) = \sum_{n=1}^{N} \tilde{w}_n(\bar{r}) A_n(\bar{t}) = \mathbf{W}^T\mathbf{A}(t), \tag{22}$$

$$\bar{u}_r^0(\bar{r}, \bar{t}) = \sum_{m=1}^{N} \tilde{u}_r^m(\bar{r}) B_m(\bar{t}) = \mathbf{U}^T\mathbf{B}(t) \tag{23}$$

where $\tilde{w}_n$ and $\tilde{u}_m$ are, respectively, orthogonal basis functions for the transverse and in-plane displacements, and A_n and B_m are amplitude parameters.

The basis function for the in-plane displacement can be determined by the linear eigenvalue problem associated with Eq. (20). Firstly, for the linear eigenvalue problem, the dimensionless vibration equation of the r axis can be written as $\frac{\partial^2 \bar{u}_r^0}{\partial \tau^2} - [\frac{\partial^2 \bar{u}_r^0}{\partial \bar{r}^2} + \frac{1}{\bar{r}}\frac{\partial \bar{u}_r^0}{\partial \bar{r}} - \frac{\bar{u}_r^0}{\bar{r}^2}] = 0$. Secondly, it is assumed that $\bar{u}_r^0 = \bar{u}_r^0 \mathrm{e}^{ik\tau}$, where k is the wave number. Finally, substituting $\bar{u}_r^0 = \bar{u}_r^0 \mathrm{e}^{ik\tau}$ into $\frac{\partial^2 \bar{u}_r^0}{\partial \tau^2} - [\frac{\partial^2 \bar{u}_r^0}{\partial \bar{r}^2} + \frac{1}{\bar{r}}\frac{\partial \bar{u}_r^0}{\partial \bar{r}} - \frac{\bar{u}_r^0}{\bar{r}^2}] = 0$, the linear eigenvalue problem can be obtained as

$$\frac{\partial^2 \bar{u}_r^0}{\partial \bar{r}^2} + \frac{1}{\bar{r}}\frac{\partial \bar{u}_r^0}{\partial \bar{r}} - \frac{\bar{u}_r^0}{\bar{r}^2} + k^2 \bar{u}_r^0 = 0. \tag{24}$$

The solution of Eq. (24) is

$$\bar{u}_r^m = B_m J_1(k_m \bar{r}) \tag{25}$$

where J_1 is a Bessel function of first kind, and the value of k_m can be determined by $J_1(k_m) = 0$.

For the transverse displacement, the same base function for transverse displacement as Meirovitch [34] is used in this Section (referring [34] for more details), which can be expressed as

$$\bar{w}_n(\bar{r}) = A_n \left[\frac{J_0(\Lambda_n \bar{r})}{J_0(\Lambda_n)} - \frac{I_0(\Lambda_n \bar{r})}{I_0(\Lambda_n)} \right] \tag{26}$$

where $I_\alpha(x) = i^{-\alpha} J_\alpha(ix)$, and the Λ_n are determined as roots of the equation $J_0(\Lambda) I_1(\Lambda) + J_1(\Lambda) I_0(\Lambda) = 0$.

The relationship between $\mathbf{B}$ and $\mathbf{A}$ can be obtained by the following: (i) substituting Eqs. (22) and (23) into Eq. (20), (ii) taking the inner product of the resulting equation with the basis function for in-plane displacement $\bar{u}_r^m$, and using the boundary conditions. As a result, the relationship between $\mathbf{B}$ and $\mathbf{A}$ is found to be

$$B_p = \mathbf{A}^T ([\mathrm{E}]_p / \Lambda) \mathbf{A} \tag{27}$$

where

$$[\mathrm{E}]_p = -\int_0^{2\pi} \int_0^1 \bar{u}_r^p \left(\frac{\partial \mathbf{W}}{\partial \bar{r}} \frac{\partial^2 \mathbf{W}^T}{\partial \bar{r}^2} + \frac{1-\nu}{2\bar{r}} \frac{\partial \mathbf{W}}{\partial \bar{r}} \frac{\partial \mathbf{W}^T}{\partial \bar{r}} \right) r \mathrm{d}r \mathrm{d}\varphi, \tag{28.1}$$

$$\Lambda = \int_0^{2\pi} \int_0^1 \left(\frac{\partial^2 \bar{u}_r^p}{\partial \bar{r}^2} + \frac{1}{\bar{r}} \frac{\partial \bar{u}_r^p}{\partial \bar{r}} - \frac{\bar{u}_r^p}{\bar{r}^2} \right) \bar{u}_r^p r \mathrm{d}r \mathrm{d}\varphi. \tag{28.2}$$

Multiplying Eq. (19.1) with $\mathbf{W}$, and substituting for $\bar{w}$ and $\bar{u}_r^0$ from Eqs. (22) and (23), integrating the resulting equation over the domain, the reduced-order model is obtained as

$$\begin{aligned} &\int \mathbf{W}\mathbf{W}^T \ddot{\mathbf{A}} r \mathrm{d}r \mathrm{d}\varphi + \left(1 + 6\chi + \bar{l}_c\right) \int \mathbf{W} \nabla^4 \mathbf{W}^T \mathbf{A} r \mathrm{d}r \mathrm{d}\varphi \\ &+ 12\alpha(1+2\chi) \int \left(\bar{\boldsymbol{\varepsilon}} + \tfrac{1}{2} \mathbf{A}^T \frac{\partial \mathbf{W}}{\partial \bar{r}} \frac{\partial \mathbf{W}^T}{\partial \bar{r}} \mathbf{A} + \nu \frac{\Upsilon}{\bar{r}} \right) \left(\frac{\partial \mathbf{W}}{\partial \bar{r}} \frac{\partial \mathbf{W}^T}{\partial \bar{r}} \right) \bar{r} \mathrm{d}r \\ &- \int (\beta_s - \beta_T) \mathbf{W} \nabla^2 \mathbf{W}^T \mathbf{A} r \mathrm{d}r \mathrm{d}\varphi - \lambda \int \frac{\mathbf{W}}{(1 - \mathbf{W}^T \mathbf{A})^2} r \mathrm{d}r \mathrm{d}\varphi - \mu \int \frac{\mathbf{W}}{(1 - \mathbf{W}^T \mathbf{A})^4} r \mathrm{d}r \mathrm{d}\varphi = 0 \end{aligned} \tag{29}$$

where $\bar{\boldsymbol{\varepsilon}} = \sum_{p=1}^{P} \mathbf{A}^T ([\mathrm{E}]_p / \Lambda) \mathbf{A} \frac{\partial \bar{u}_r^p}{\partial \bar{r}}$ and $\Upsilon = \sum_{p=1}^{P} \mathbf{A}^T ([\mathrm{E}]_p / \Lambda) \mathbf{A} \bar{u}_r^p$.

Using the divergence theorem and imposing boundary conditions, it was obtained

$$\mathbf{m}\ddot{\mathbf{A}} + [(1 + 6\chi + \bar{l}_c)\mathbf{k}_1 + (\beta_s - \beta_T)\mathbf{k}_2 + \alpha(1+2\chi)\mathbf{k}_3(\mathbf{A})]\mathbf{A} - \lambda \mathbf{f}_e - \mu \mathbf{f}_c = 0 \tag{30}$$

where

$$\mathbf{m} = 2\pi \int_0^1 \mathbf{W}\mathbf{W}^T \bar{r} \mathrm{d}\bar{r}, \tag{31.1}$$

$$\mathbf{k}_1 = 2\pi \int_0^1 \left(\frac{1}{\bar{r}} \frac{\partial \mathbf{W}}{\partial \bar{r}} \frac{\partial \mathbf{W}^T}{\partial \bar{r}} + r \frac{\partial^2 \mathbf{W}}{\partial \bar{r}^2} \frac{\partial^2 \mathbf{W}^T}{\partial \bar{r}^2} \right) \mathrm{d}\bar{r}, \tag{31.2}$$

$$\mathbf{k}_2 = 2\pi \int_0^1 \frac{\partial \mathbf{W}}{\partial \bar{r}} \frac{\partial \mathbf{W}^T}{\partial \bar{r}} \bar{r} \mathrm{d}\bar{r}, \tag{31.3}$$

$$\mathbf{k}_3 = 24\pi \int \left(\bar{\boldsymbol{\varepsilon}} + \frac{1}{2} \mathbf{A}^T \frac{\partial \mathbf{W}}{\partial \bar{r}} \frac{\partial \mathbf{W}^T}{\partial \bar{r}} \mathbf{A} + \nu \frac{\Upsilon}{\bar{r}} \right) \left(\frac{\partial \mathbf{W}}{\partial \bar{r}} \frac{\partial \mathbf{W}^T}{\partial \bar{r}} \right) \bar{r} \mathrm{d}r, \tag{31.4}$$

$$\mathbf{f}_e(\mathbf{A}) = 2\pi \int_0^1 \frac{\mathbf{W}}{(1 - \mathbf{W}^T\mathbf{A})^2} \bar{r} \mathrm{d}\bar{r}, \tag{31.5}$$

$$\mathbf{f}_c(\mathbf{A}) = 2\pi \int_0^1 \frac{\mathbf{W}}{(1 - \mathbf{W}^T\mathbf{A})^4} \bar{r} \mathrm{d}\bar{r}. \tag{31.6}$$

In Eq. (30), $\mathbf{k}_1$ is the linear stiffness matrix, $\beta_s \mathbf{k}_2$ and $\beta_T \mathbf{k}_2$ are the stiffness matrices contributed by surface energy and temperature change, $\mathbf{k}_3(\mathbf{A})$ represents the nonlinear stiffness matrix contributed by geometrically nonlinear deformation. It is noted that when α approaches zero, the nonlinear stiffness $\mathbf{k}_3(\mathbf{A})$ approaches zero and can be neglected. At this situation, Eq. (30) can be reduced to $\mathbf{m}\ddot{\mathbf{A}} + [(1 + 6\chi + \bar{l}_c)\mathbf{k}_1 + (\beta_s - \beta_T)\mathbf{k}_2]\mathbf{A} - \lambda \mathbf{f}_e - \mu \mathbf{f}_c = 0$, which is the motion equation of linear plates.

The natural frequencies of the deflected circular plate at a given situation ($\mathbf{A}, \chi, \beta_s, \beta_T, \lambda, \mu, \bar{l}_c$) can be determined by the following procedure [9]. We perturb the equilibrium state A with a harmonic term e^{iwt} as $A + \bar{A}\mathrm{e}^{iwt}$, where A is a constant such that $|\bar{A}| << |A|$ and $i = \sqrt{-1}$. Substituting $A + \bar{A}\mathrm{e}^{iwt}$ into Eq. (30) and retaining terms linear in A, one obtains the following relation for the natural frequency:

$$\det(\mathbf{K}(\mathbf{A}, \chi, \beta_s, \beta_T, \lambda, \mu, \bar{l}_c) - \omega^2 \mathbf{m}) = 0 \tag{32}$$

where

$$\mathbf{K}(\mathbf{A}, \chi, \beta_s, \beta_T, \lambda, \mu, \bar{l}_c) = [(1 + 6\chi + \bar{l}_c)\mathbf{k}_1 + (\beta_s - \beta_T)\mathbf{k}_2 + 3\alpha(1 + 2\chi)\mathbf{k}_3(\mathbf{A})] - \lambda \frac{d\mathbf{f}_e(\mathbf{A})}{d\mathbf{A}} - \mu \frac{d\mathbf{f}_c(\mathbf{A})}{d\mathbf{A}}. \tag{33}$$

Since $\det[\mathbf{K}(\mathbf{A}, \chi, \beta_s, \beta_T, \lambda, \mu, \bar{l}_c)] = 0$ at pull-in, it follows that at least one natural frequency of the switch is zero, when pull-in occurs. This also provides a useful way to find the pull-in parameters of the electrostatically actuated plate.

4 Numerical results and discussion

Figure 2 shows the convergence of the presented model. It is found that the convergence results can be obtained by using the 21×21 Gauss quadrature rule. Therefore, the integrals appearing in this paper are evaluated using the 21×21 Gauss quadrature rule. In the following Figures, ω_0 is the fundamental frequency of a clamped circular plate with $V = 0$, $l_c = 0$, $E^s = 0$, and $\gamma_0 = 0$. The value of ω_0 obtained by the present model with $n = 3$ and $m = 4$ is 10.2 which matches well with the values reported by Batra et al. [9].

The material properties of silver are $E = 76$ Gpa, $\nu = 0.3$, $E^s = 1.22$ N/m and $\gamma_0 = 0.89$ N/m [35,36]. Figure 3 shows the variation of the normalized frequencies of the circular micro-/nanoplate with applied voltage for different material length scale parameters. It can be seen that the classical theory (without consideration of the effect of material length scale) makes a lower prediction of the frequency. The normalized frequency increases with increasing material length scale. This phenomenon can be explained by Eq. (26), which suggests that the material length scale increases the stiffness matrix. The influence of the material length scale on the normalized frequency increases with decreasing thickness h. Equation $\bar{l}_c = 6(1 - \nu)(l_c/h)^2$ can be used to explain this phenomenon. Keeping l_c as a constant, decreasing the thickness h increases the parameter $\bar{l}_c$ and then increases the stiffness matrix. It is also found that the normalized frequencies rapidly decrease to zeros,

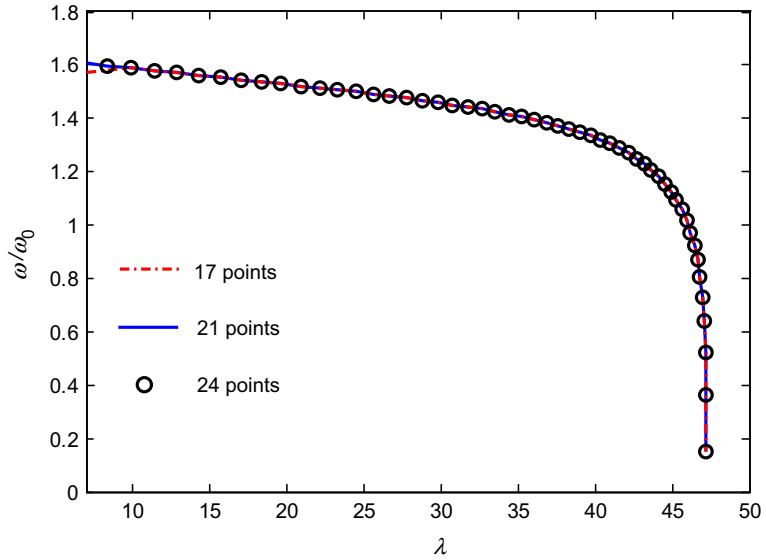

Fig. 2 Variation of the normalized frequency of the circular micro-/nanoplate with the applied voltage for different Gauss quadrature rules ($h = 500$ nm, $R = 100$ h, $g_0 = 2$ h, $\bar{l}_c = 1/4$ and $\Delta T = -100$ K)

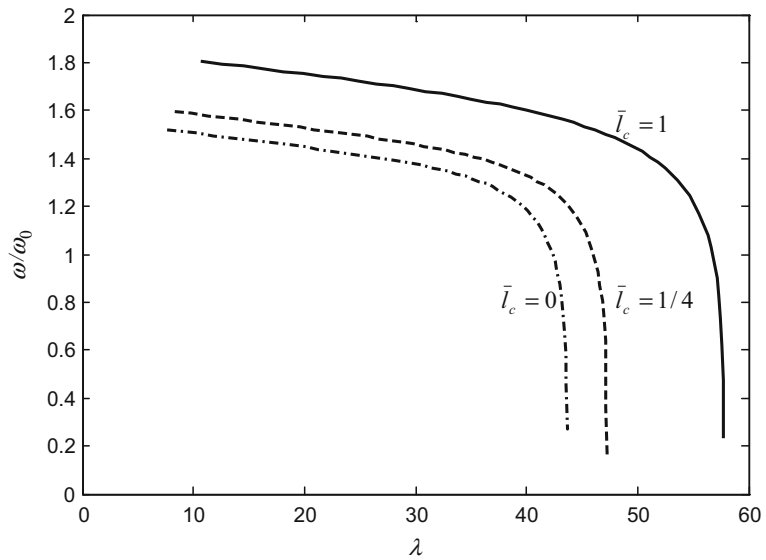

Fig. 3 Variation of the normalized frequency of the circular micro-/nanoplate with the applied voltage for different material length scale parameters $\bar{l}_c$ ($h = 500$ nm, $R = 100$ h, $g_0 = 2$ h and $\Delta T = -100$ K)

when the applied voltage (λ) comes close to a critical value, which is defined as the pull-in voltage, denoted by λ_{PI}. In addition, the material length scale also increases the pull-in voltage of the circular plate.

The variation of normalized frequencies of the circular micro-/nanoplate with applied voltage for different thickneses is plotted in Fig. 4. Comparing the results with and without surface energy, it is found that surface energy increases the normalized frequencies of the circular plate. The influence of surface energy on the normalized frequencies becomes significant if the thickness of the plate decreases. The reason for this is that the surface energy enhances the plate stiffness, and the ratio of surface energy to bulk energy increases with decreasing plate thickness. The difference between the presented model with and without surface energy becomes large when the applied voltage increases. It is also found that the surface energy increases the pull-in voltage of the circular micro-/nanoplate.

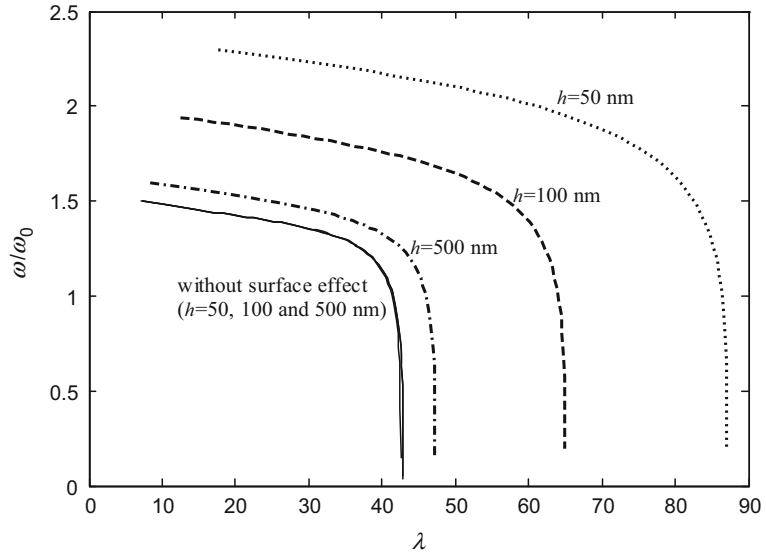

Fig. 4 Variation of the normalized frequency of the circular micro-/nanoplate with the applied voltage for different thickneses ($R = 100$ h, $g_0 = 2$ h, $\bar{l}_c = 1/4$ and $\Delta T = -100$ K)

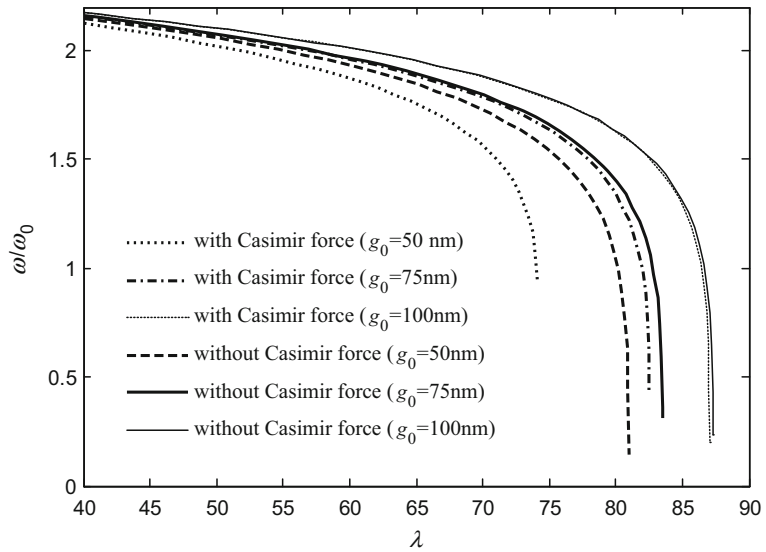

Fig. 5 Variation of the normalized frequency of the circular micro-/nanoplate with the applied voltage for different initial gaps g_0 ($h = 50$ nm, $R = 100$ h, $\bar{l}_c = 1/4$ and $\Delta T = -100$ K)

Figure 5 plots the normalized frequency of the circular micro-/nanoplate for different initial gaps g_0. It is found that Casimir forces enlarge the force matrix, and decrease the frequencies and pull-in voltages of the plate. The influence of Casimir force on frequencies decreases with increasing initial gap g_0. The relationship $\mu = \bar{h}c\pi^2 h(l/h)^4(1-\upsilon^2)/(20Eg_0^5)$ can explain this phenomenon. From this relation, it can be found that increasing the initial gap g_0 decreases the value of μ. If the initial gap g_0 reaches a certain value, the value of μ will approach to zero. At this situation, the effect of Casimir force can be neglected.

Figure 6 makes comparisons of the results based on linear and nonlinear theories. It can be seen that the frequencies predicted by the nonlinear theory are higher than those predicted by the linear theory. The fact is that the effect of strain hardening increases the stiffness matrix. The effect of geometrically nonlinear strain on the frequencies rapidly increases with increasing parameter $\alpha = (g_0/h)^2$, due to the fact that the nonlinear stiffness matrix $\alpha(1+2\chi)\mathbf{k}_3$ increases with increasing parameter α. The geometrically nonlinear strain also

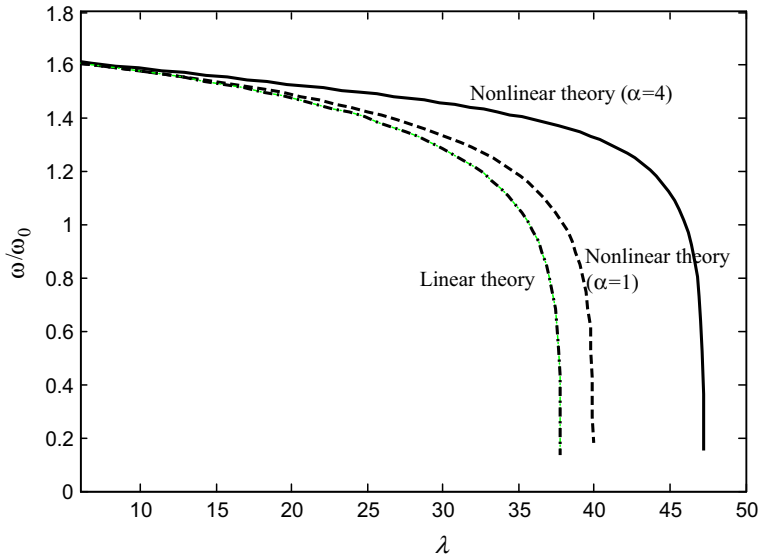

Fig. 6 Variation of the normalized frequency of the circular micro-/nanoplate with the applied voltage based on linear and nonlinear theories ($h = 500$ nm, $R = 100$ h, $\bar{l}_c = 1/4$ and $\Delta T = -100$ K)

increases the pull-in voltages. Once again, the difference between the nonlinear and linear results becomes large when the applied voltage increases.

Figure 7 shows the variation of the normalized frequency of the circular micro-/nanoplate with the applied voltage for different temperature changes. In Fig. 7, we just assumed a temperature change to investigate the effect of the temperature variation. Both positive and negative temperature variation can be emerged in real applications, for example, nanodevices may be subjected to positive temperature changes during sensing operation and negative temperature changes during device packaging. When the temperature change is positive, the normalized frequency is smaller than that without temperature change. If the temperature change is negative, the normalized frequency is larger than that without temperature change. The reason for this is that a positive temperature change induces an additional compressive force, which makes the plate softer. A negative temperature change induces an additional tensile force which makes the plate stiffer. From the relationship$\beta_{\mathrm{T}} = 12(1+\nu)(1+2\chi)(R/h)^2\alpha_{\mathrm{T}}\Delta T$, it can be seen that the effect of the temperature change on the normalized frequency increases with increasing radius to thickness ratio. It is also observed that a positive temperature change decreases the pull-in voltages, a negative temperature change increases pull-in voltages. Moreover, the trend of the curves corresponding to positive temperatures (ΔT in the range of 0K to 137K, as shown in Fig. 7b) is nonmonotonic due to the combined effect of the stiffening effect introduced by mid-plane stretching and surface energy, and the softening effect introduced by positive temperature change, electric, and Casimir forces. It is noted that in absence of an applied voltage the buckling temperature of the circular nanoplate is $\Delta T = 137K$. The frequency of the circular plate corresponding to the buckling temperature is zero. The monotonic trend of curves implies that the softening effect is always lager than the stiffening effect.

5 Conclusions

The effects of surface energy, Casimir forces and temperature change on the nonlinear resonant behavior of electrostatically actuated circular micro-/nanoplates are studied, based on the modified couple stress theory. The nonlinear motion equation of an electrostatically actuated circular micro-/nanoplate is derived by using Hamilton's principle. The reduced-order model incorporating the material length scale, geometrically nonlinear strain, surface energy, and temperature change is derived and solved numerically. Results show that material length scale, surface energy, negative temperature change, and geometry nonlinear strain increase frequency and pull-in voltage of the circular micro-/nanoplate. However, Casimir force reduces the frequency of the micro-/nanoplate. The effects of surface energy and material length scale on frequency become more obvious

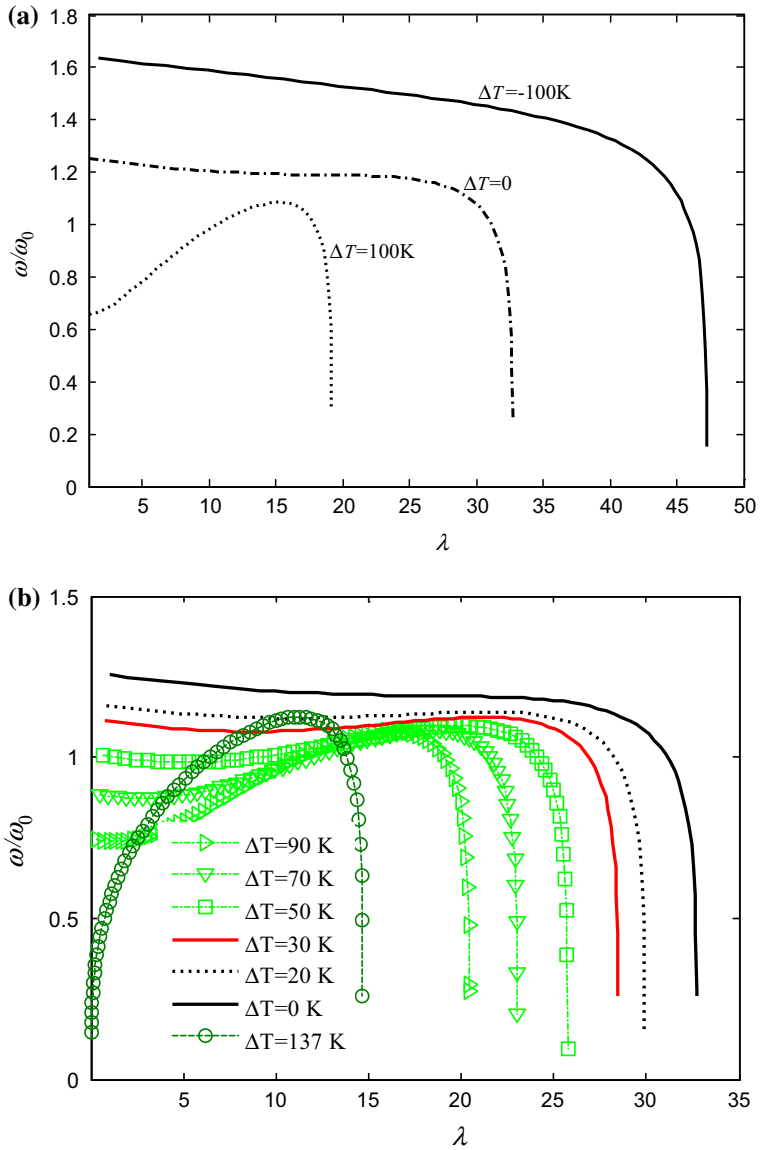

Fig. 7 Variation of the normalized frequency of the circular micro-/nanoplate with the applied voltage for different temperature changes ($h = 500$ nm, $R = 100$ h, $g_0 = 2$ h and $\bar{l}_c = 1/4$)

for a thinner plate. The influence of the geometrically nonlinear strain on frequencies is more significant for a large initial gap to thickness ratio of the plate.

Acknowledgements This research was supported by the Natural Science Foundation of Guangdong Province of China (project nos. 2016A030310367, 2016A030311006), Research Innovation Fund of Shenzhen City of China (project no. JCYJ20150805142729431, JCYJ20160427184645305), the National Natural Science Foundation of China (project nos. 1167020127, 11372086, 1160020094), and China Postdoctoral Science Foundation Funded Special Project (project no.2016T90275).

References

1. Pelesko, J.A., Bernstein, D.H.: Modeling MEMS and NEMS, Chap. 7. Chapman & Hall, Boca Raton (2002)
2. Nguyen, C.T.C., Katehi, L.P.B., Rebeiz, G.M.: Micromachined devices for wireless communications. Proc. IEEE **86**, 1756–1768 (1998)
3. Gupta, R.K., Senturia, S.D.: Pull-in time dynamics as a measure of absolute pressure. In: Proceedings IEEE International Workshop on Microelectromechanical Systems (MEMS'97), Nagoya, Japan, pp. 290–294 (1997)

4. Sheikhlou, M., Shabani, R., Rezazadeh, G.: Nonlinear analysis of electrostatically actuated diaphragm-type micropumps. Nonlinear Dyn. **83**, 951–961 (2016)
5. Howe, R.T., Muller, R.S.: Resonant-microbridge vapor sensor. IEEE Trans. Electron. Devices **33**, 499–506 (1986)
6. Ramezani, A., Alasty, A., Akbari, J.: Closed-form solutions of the pull-in instability in nano-cantilevers under electrostatic and intermolecular surface forces. Int. J. Solids Struct. **44**, 4925–4941 (2007)
7. Jia, X.L., Yang, J., Kitipornchai, S.: Pull-in instability of geometrically nonlinear micro-switches under electrostatic and Casimir forces. Acta Mech. **218**, 161–174 (2011)
8. Jia, X.L., Yang, J., Kitipornchai, S., Lim, C.M.: Free vibration of geometrically nonlinear micro-switches under electrostatic and Casimir forces. Smart Mater. Struct. **19**, 115028 (2010)
9. Batra, R.C., Porfiri, M., Spinello, D.: Reduced-order models for microelectromechanical rectangular and circular plates incorporating the Casimir force. Int. J. Solids Struct. **45**, 3558–3583 (2008)
10. Batra, R.C., Porfiri, M., Spinello, D.: Effect of van der Waals force and thermal stress on pull-in instability of microplates. Sensors **8**, 1048–1069 (2008)
11. Batra, R.C., Porfiri, M., Spinello, D.: Vibrations and pull-in instabilities of microelectromechanical von Kármán elliptic plates incorporating the Casimir force. J. Sound Vib. **315**, 939–960 (2008)
12. Wang, Y.G., Lin, W.H., Li, X.M., Feng, Z.J.: Bending and vibration of an electrostatically actuated circular microplate in presence of Casimir force. Appl. Math. Model. **35**, 2348–2357 (2011)
13. Gurtin, M.E., Murdoch, A.I.: A continuum theory of elastic material surfaces. Arch. Ration. Mech. Anal. **57**, 291–323 (1975)
14. Fu, Y., Zhang, J.: Size-dependent pull-in phenomena in electrically actuated nanobeams incorporating surface energies. Appl. Math. Model. **35**, 941–951 (2011)
15. Hosseini-Hashemi, S., Nahas, I., Fakher, M., Nazemnezhad, R.: Surface effects on the free vibration of piezoelectric functionally graded nanobeams using nonlocal elasticity. Acta Mech. **225**, 1555–1564 (2014)
16. Sahmani, S., Aghdam, M.M., Bahrami, M.: On the free vibration characteristics of postbuckled third-order shear deformable FGM nanobeams including surface effects. Compos. Struct. **121**, 377–385 (2015)
17. Yang, F., Chong, A.C.M., Lam, D.C.C., Tong, P.: Couple stress based strain gradient theory for elasticity. Int. J. Solids Struct. **39**, 2731–2743 (2002)
18. Thai, H.T., Vo, T.P., Nguyen, T.K., Lee, J.: Size-dependent behavior of functionally graded sandwich microbeams based on the modified couple stress theory. Compos. Struct. **123**, 337–349 (2015)
19. Romanoff, J., Reddy, J.N.: Experimental validation of the modified couple stress Timoshenko beam theory for web-core sandwich panels. Compos. Struct. **111**, 130–137 (2014)
20. Farokhi, H., Ghayesh, M.H.: Nonlinear dynamical behaviour of geometrically imperfect microplates based on modified couple stress theory. Int. J. Mech. Sci. **90**, 133–144 (2015)
21. Gao, X.L., Mahmoud, F.F.: A new Bernoulli–Euler beam model incorporating microstructure and surface energy effects. Z. Angew. Math. Phys. **65**, 393–404 (2014)
22. Mahmoud, F.F., Eltaher, M.A., Alshorbagy, A.E., Meletis, E.: Static analysis of nanobeams including surface effects by nonlocal finite element. J. Mech. Sci. Technol. **26**, 3555–3563 (2012)
23. Shaat, M., Mahmoud, F.F., Gao, X.L., Faheem, A.F.: Size-dependent bending analysis of Kirchhoff nano-plates based on a modified couple-stress theory including surface effects. Int. J. Mech. Sci. **79**, 31–37 (2014)
24. Wang, K.F., Kitamura, T., Wang, B.: Nonlinear pull-in instability and free vibration of micro/nanoscale plates with surface energy-a modified couple stress theory model. Int. J. Mech. Sci. **99**, 288–296 (2015)
25. Zhu, Y., Espinosa, H.D.: Reliability of capacitive RFMEMS switches at high and low temperatures. Int. J. RF Microw. Comput. Aided Eng. **14**, 317–328 (2004)
26. Nakhaie, J.G.: Mathematical modeling and simulation of thermal effects in flexural microcantilever resonator dynamics. J. Vib. Control **12**, 139–163 (2006)
27. Zhu, Y., Espinosa, H.D.: Effect of temperature on capacitive RF MEMS switch performance—a coupled-field analysis. J. Micromech. Microeng. **14**, 1270–1279 (2004)
28. Nayfeh, A.H., Younis, M.I.: Modeling and simulations of thermoelastic damping in microplates. J. Micromech. Microeng. **14**, 1711–1717 (2004)
29. Mohammadi, V., Ansari, R., Faghih, S.M., Gholami, R., Sahmani, S.: Size-dependent dynamic pull-in instability of hydrostatically and electrostatically actuated circular microplates. Nonlinear Dyn. **73**, 1515–1526 (2013)
30. Vogl, G.W., Nayfeh, A.H.: Primary resonance excitation of electrically actuated clamped circular plates. Nonlinear Dyn. **47**, 181–192 (2007)
31. Ru, C.Q.: Simple geometrical explanation of Gurtin–Murdoch model of surface elasticity with clarification of its related versions. Sci. China Phys. Mech. Astron. **53**, 536–544 (2010)
32. Bordag, M.: Casimir effect for a sphere and a cylinder in front of a plane and corrections to the proximity force theorem. Phys. Rev. D **73**, 125018 (2006)
33. Gies, H., Klingmuller, K.: Casimir effect for curved geometries: proximity-force-approximation validity limits. Phys. Rev. Lett. **96**, 220401 (2006)
34. Meirovitch, L.: Analytical Methods in Vibrations. Macmillan, New York (1967)
35. Wang, G.F., Feng, X.Q.: Effects of surface elasticity and residual surface tension on the natural frequency of microbeams. Appl. Phys. Lett. **90**, 231904 (2007)
36. Shenoy, V.B.: Atomistic calculations of elastic properties of metallic fcc crystal surfaces. Phys. Rev. B **71**, 094104 (2005)